Journal of Mines, Metals and Fuels, *71(12A): 312-325; 2023. DOI: 10.18311/jmmf/2023/43608*

Print ISSN : 0022-2755

Journal of Mines, Metals and Fuels

**Contents available at:** *www.informaticsjournals.com/index.php/jmmf*

# A Generalized Mathematical Model to Predict Core Loss of 15kw 3Φ-Squirrel Cage Induction Motor at Various Load for Industrial Applications

**S. Sachin[1]*, Krishnan Manickavasagam[2] and A. T. Sriram[3]**

*[1]Department of Electrical Engineering, M. S. Ramaiah University of Applied Sciences, Bengaluru - 560054, Karnataka, India; sachins.schns@gmail.com*

*[2]Department of Electrical and Electronics Engineering Education, National Institute of Technical Teachers Training and Research, Bhopal - 462 002, Madhya Pradesh, India; kmanickavasagam@nitttrbpl.ac.in*

*[3]Department of Automotive and Aeronautical Engineering, M. S. Ramaiah University of Applied Sciences, Bengaluru - 560054, Karnataka, India; atsriram.aae.et@msruas.ac.in*

## Abstract

*The demand for effective operation of induction motor has become necessary in industrial, domestic, manufacturing, excavation, mines and many other applications. Losses estimation of the Induction Motor play a very important role in analyzing the electrical and thermal performances. Traditionally copper loss is estimated using load current and core losses is assumed constant, as it is difficult to measure core loss. An additional sensor must be place in air gap of the motor to measure core loss, increasing the complexity and uneconomical. Hence in this paper, a Finite Element Method (FEM) is used to estimate the core losses on 3ϕ - 15kW Squirrel Cage Induction Motor (SCIM) at various load conditions. A generalized mathematical model is needed to predict the core loss of the motor at various load conditions. Hence a generalized mathematical model proposed using regression technique is validated with conventional approach.*

**Keywords:** *Core Loss, Finite Element Method (FEM), Squirrel Cage Induction Motor (SCIM)*

## 1.0 Introduction

The demand for effective operation of induction motor has become necessary in industrial, domestic, manufacturing, excavation, mines and many other applications. The SCIM meet all necessities of small - large scale industries. The inner parts of SCIM are stator and rotor. The main problem in is rise in temperature in its parts. When SCIM is working continuously, the temperature rise may cross the thermal limit, leading to failure. The failure in stator and rotor of SCIM is more than 70%. Rotor bras and stator conductors will collapse due to high temperature rise. Temperature rise of SCIM becomes a primary technical challenge in design of SCIM. In design process it is essential to know the temperature rise in major part of SCIM[1-5].

SCIM's are typical used in industrial applications, because of its rugged construction and low cost. One of the major reason for temperature rise is loss dissipation. The loss dissipation in SCIM increases the temperature in various parts, viz. stator windings, rotor bars, and motor outer frame etc. The heat generated in SCIM can be extracted via conduction, convection and radiation. The SCIM can be protected from high temperature

**Author for correspondence*

rise, by reducing losses and by providing cooling system[6-10].

Thermal analysis of SCIM is more important compared to Electro-Magnetic Analysis (EMA) as it is dependent on material properties and on the manufacturing (MirceaPopescu, 2014). The heat contribution of rotor in SCIM is 5% from rotor iron losses and 15% from rotor copper loss, 20% from stator iron loss, 40% from stator copper loss, mechanical losses and stray losses contributes 20%[11-17].

In this work, a 15 kW, 3ϕ-SCIM is used to estimate the value of core loss. A 2D FEM model of 3ϕ-SCIM is developed, to estimate the core loss at different loads under condition at ambient temperature of 25˚C.

The objective of this paper are:

- Estimation of Losses of SCIM using conventional method (Constant Core Loss)
- Estimation of core loss from No-load to over load condition
- To arrive at a generalized mathematical model to predict core loss of 15kW 3ϕ-SCIM

## 2.0 Loss Estimation of 3ϕ - SCIM

The copper loss is calculated with regard to load current according to the conventional method. The mechanical losses and stray losses is calculated. To calculate core loss, which is considered to be constant for all load circumstances, the total of all expected losses is subtracted from the rated loss of the IM. The power flow diagram of SCIM is as shown in Figure 1.

The equations used to evaluate the losses are as follows:

The input power of the stator:

$$P_1 = \sqrt{3} * V_{line} * I_{line} * \cos\emptyset \quad (1)$$

The magnetization current is neglected.

$$I_1 = I_2' \quad (2)$$

The synchronous speed is given by:

$$N_s = \frac{120 * f}{p}, \qquad \omega_s = \frac{2 * \pi * N_s}{60} \quad (3)$$

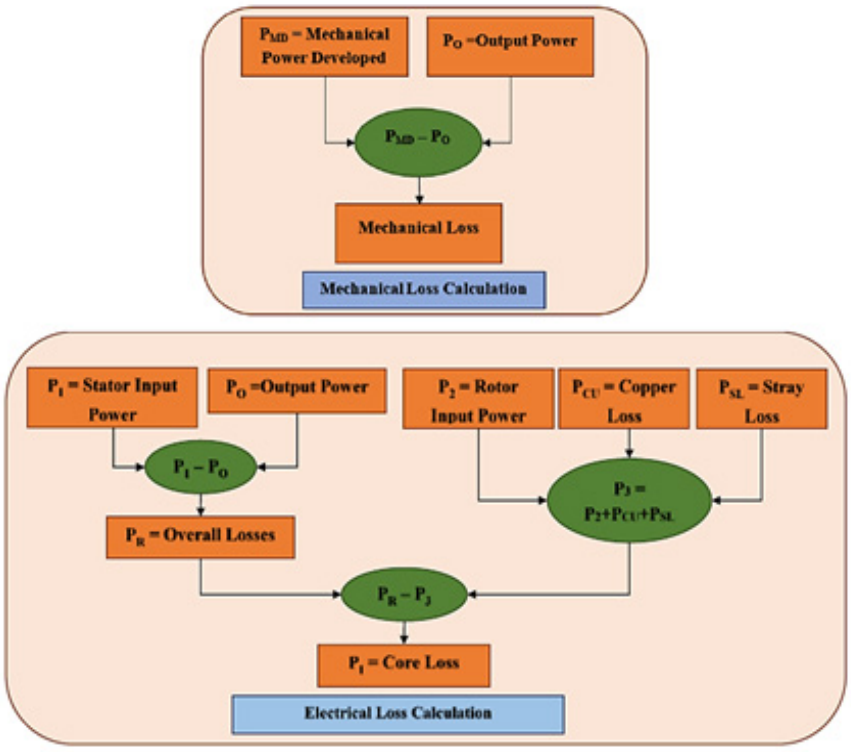


**Figure 1.** Power flow diagram of SCIM.

The Slip

$$N = (1 - S)N_s \quad (4)$$

The copper loss at stator is given by:

$$P_{cu} = 3 * (I_L)^2 * R_s \quad (5)$$

The input power at rotor is estimated using:

$$P_2 = \omega_s * T \quad (6)$$

The Al losses at rotor is estimated using:

$$P_{Al}\ 3 * I_2'^2 * r_2' = S * P_2 \quad (7)$$

Mechanical power developed is given by:

$$P_m = (1 - S) * P_2 \quad (8)$$

Losses (Mechanical)

$$P_m = P_o + \text{Mechanical losses} \quad (9)$$

The total core losses is estimated by:

$$P_1 = P_2 + P_{cu} + P_{iron} + \text{Additional losses} \quad (10)$$

At all the load conditions core loss is assumed constant. The Table 1 contains the SCIM's specs. The calculated losses of 15kW 3ϕ - SCIM at full load condition is listed in Table 2.

**Table 1.** Specification of 15kW 3ϕ - SCIM

| Parameters | Parameters 15kW SCIM |
|---|---|
| Rated Supply Voltage | 415 V |
| Rated Line Current | 28.18 A |
| Current at No-load | 11.72 A |
| Rated Power | 15 kW |
| Number of Pole | 4 |
| Rated Speed of Motor | 1462 RPM |
| Motor Speed at No-load | 1488 RPM |
| Motor Efficiency | 90% |
| Torque | 97.98 N-m |
| Ambient Temperature | 25˚C |

**Table 2.** Losses in 15 kW 3ϕ - SCIM

| Loss Label | Losses (W) |
|---|---|
| Iron Losses | 310.5 |
| Stator Copper Losses | 654.2 |
| Rotor Aluminum Losses | 409.7 |
| Additional Losses | 199.9 |
| Losses at Rated Load | 1658 |
| Losses at No-load | 517 |

IM functionality in real time the core loss will change depending on the load circumstances. Unfortunately, it is very challenging to calculate the core losses. An additional flux sensing sensors has to be connected in the air gap to obtain the values of flux density and in turn the core losses, making it expensive and complex. Based on this challenge, a 2D FEM model is created to calculate the core loss on IM (Variable Core Loss) described in session 3.

## 3.0 Variable Core Loss - FEM Approach

To measure the magnetic flux density an additional instrument has to be constructed but it's not easy in air gap. The core loss is dependent on the flux density values and can be predicted using computational techniques. For 3ϕ-SCIM, a stator and rotor 2D FEM model is created and meshed. The data used to calculate the magnetic flux density is the load currents[4].

### 3.1 2D Modelling of 3ϕ-SCIM

Stator, rotor and shaft are engaged in construction and modelling of 3ϕ-SCIM. Figure 2 depicts the stator's construction and specifications. Figure 3 depicts the design specs for the rotor, rotor bars, and rotor. Figure 4 depicts the assembled 2D Stator, Rotor design, and

assembled model of the SCIM. To calculate the magnetic flux density, the material characteristics are assigned, meshed, and simulated.

## 3.2 Estimation of Magnetic Flux Density using 2D Model

Point assessment/evaluation method is used to determine

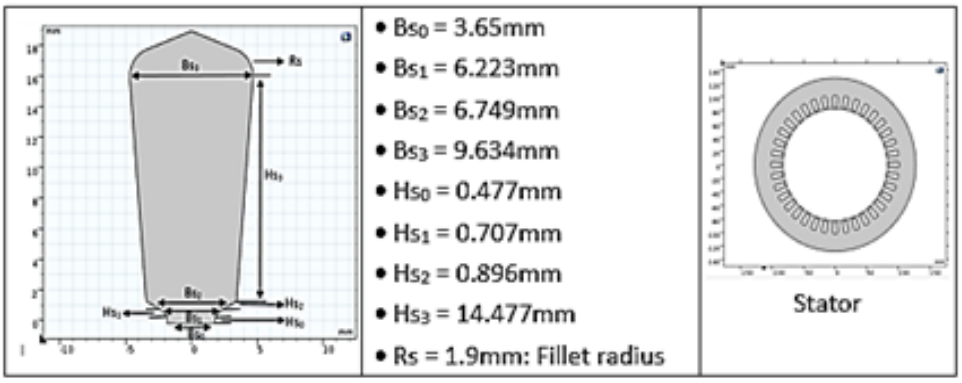


**Figure 2.** 2D model of the stator.

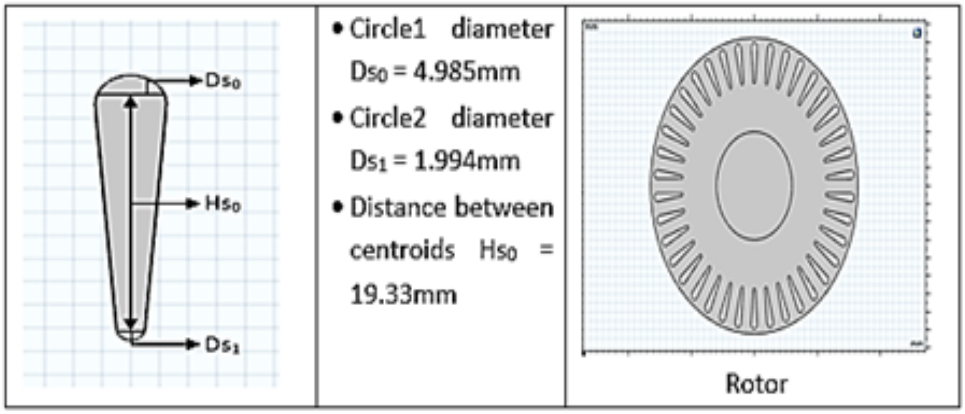


**Figure 3.** 2D model of the rotor.

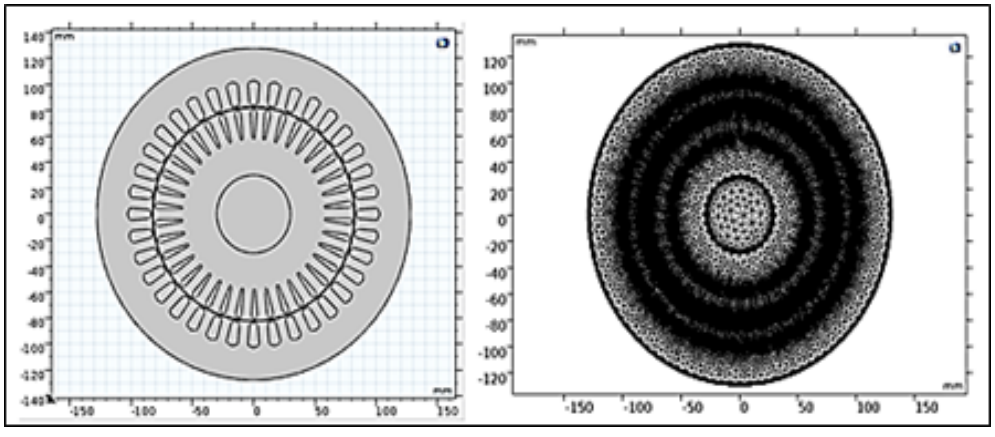

**Figure 4.** Assembled 2D stator rotor design and meshed model.

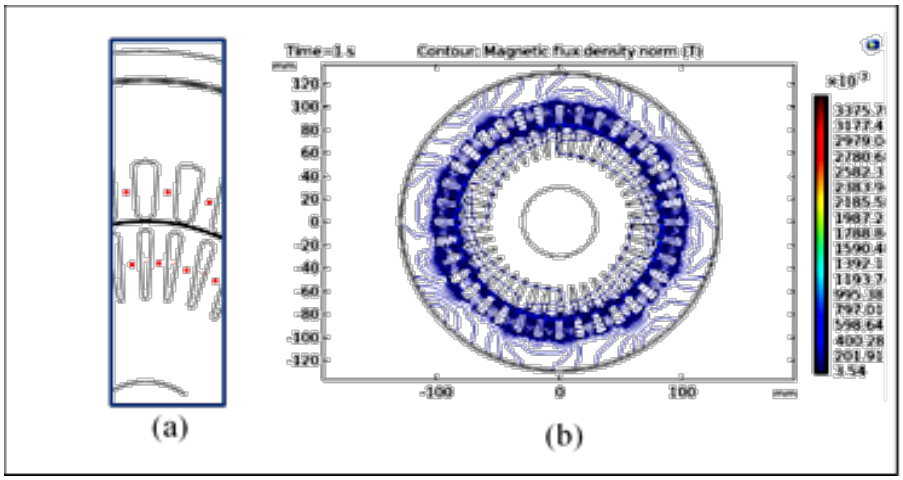


**Figure 5.** **a.** Cut view of point evaluation, **b.** Magnetic flux density counter plot.

the magnetic flux density in rotor and stator of the SCIM. To conduct out point evaluation, cut spots are marked on the stator and rotor as shown in Figure 5a. Magnetic flux density counter plot is as shown in Figure 5b.

For different load circumstances/loads, the magnitude of flux density at the core of the stator and rotor is calculated and is listed in Table 3. Table 4 lists the estimated stator and rotor core losses under various load conditions.

The core/iron losses in 3ϕ-SCIM is mainly classified into hysteresis losses (Phys), and eddy-current losses (Peddy). There is an additional component to the core loss that can be considered as in the Bertotti's model to make the core loss more accurate[6].

This additional loss is not considered here to make analysis simple. Individually Phys and Peddy increase with change in frequency and load, equations are given by equation 11 and equation 12. The estimated Phys and Peddy losses at 50Hz, at various load condition is as tabulate in Table 4.

$$P_{hys} = k_h f B_m^{1.6} \tag{11}$$

$$P_{eddy} = k_e f^2 B_m^2 \tag{12}$$

$$P_{core} = P_{hys} + P_{eddy} \tag{13}$$

From equations it is evident that the values of core losses are dependent on the values of flux density and frequency.

## 4.0 Regression Analysis

Regression analysis, a statistical tool, is a method used to forecast the parameter of a system. At any operating situation, the parameter can be anticipated using linear equations without any power loss or time. Regression analysis is used to enhance the performance and dependability of the system. Regression analysis of each system component yields the generalized equation. Regression analysis is used to create the regression model.

The generalized mathematical equation for magnetic flux density at stator core, and rotor core are obtained using linear regression analysis, the resulting the equations of stator core, and rotor core of the SCIM as follows:

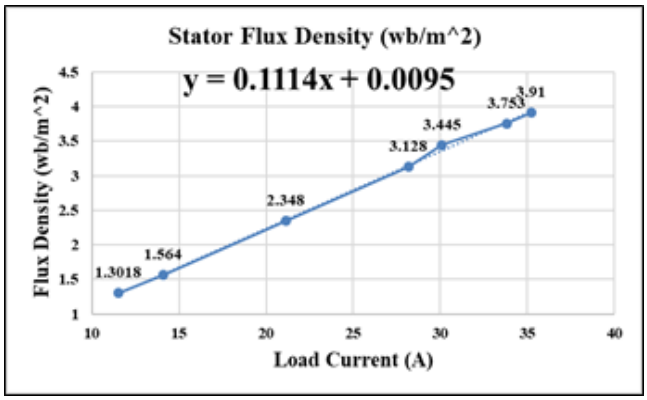


**Figure 6.** Regression analysis for stator flux density.

**Table 3.** Estimated magnetic flux density of SCIM

| Load Conditions | Load Current (A) | Stator Flux Density (Wb/m$^2$) | Rotor Flux Density (Wb/m$^2$) |
|---|---|---|---|
| No-Load | 11.50 | 1.3018 | 0.1386 |
| Half Load | 14.09 | 1.564 | 0.1722 |
| 3/4$^{th}$ Load | 21.13 | 2.348 | 0.2608 |
| Full Load | 28.18 | 3.128 | 0.3528 |
| 110% Load | 30.10 | 3.445 | 0.3864 |
| 120% Load | 33.81 | 3.753 | 0.4158 |
| 125% Load | 35.22 | 3.910 | 0.4284 |

**Table 4.** Variable core loss of 15kW SCIM

| Load Conditions | Load Current (A) | Stator Core Loss (W) | Rotor Core Loss (W) | Total Core Loss (W) |
|---|---|---|---|---|
| No - Load | 11.50 | 76.54 | 0.0025 | 76.54 |
| Half Load | 14.09 | 102.69 | 0.0427 | 102.74 |
| 3/4th Load | 21.13 | 197.00 | 0.1427 | 197.14 |
| Full Load | 28.18 | 311.73 | 0.3575 | 312.09 |
| 110% Load | 30.10 | 363.94 | 0.4800 | 364.42 |
| 120% Load | 33.81 | 417.50 | 0.6039 | 418.10 |
| 125% Load | 35.22 | 445.72 | 0.6680 | 446.39 |

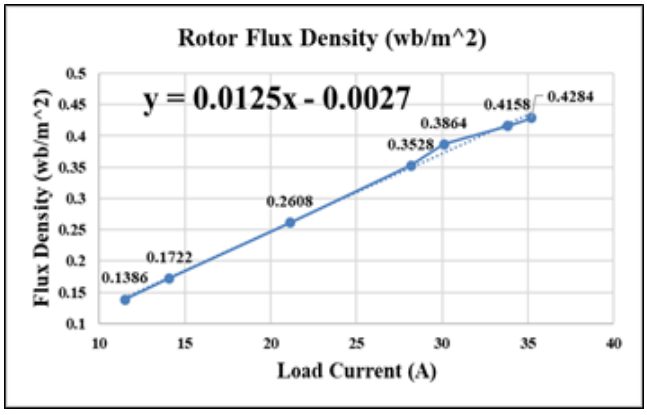


**Figure 7.** Regression analysis for rotor flux density.

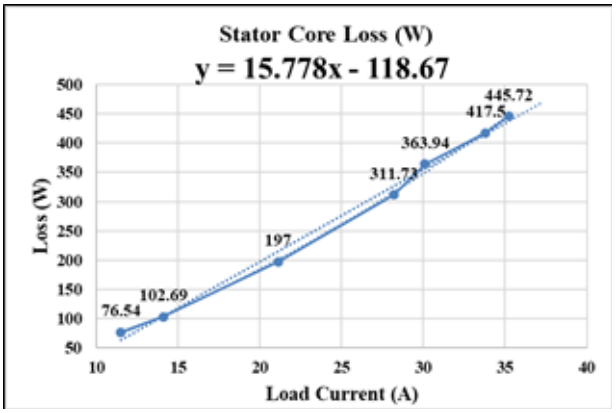


**Figure 8.** Regression analysis of stator core loss.

Generalized regression equation for stator core,

$$y = 0.1114*x + 0.0095 \quad (14)$$

Generalized regression equation for rotor core,

$$y = 0.0125*x + 0.0027 \quad (15)$$

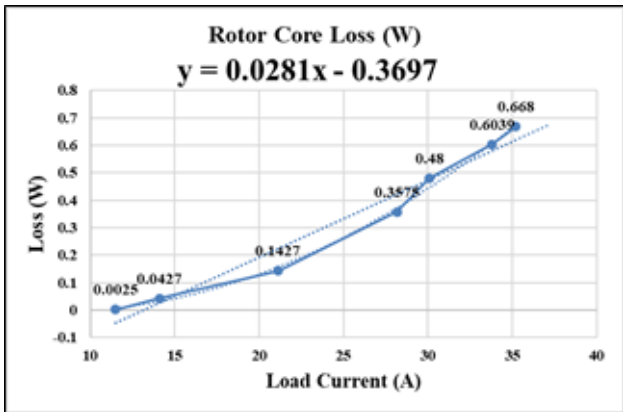


**Figure 9.** Regression analysis of rotor core loss.

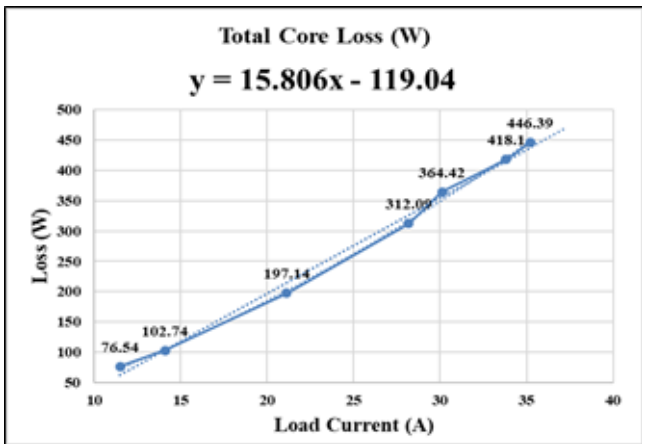


**Figure 10.** Regression analysis of total core loss.

Here, 'y' gives magnetic flux density and 'x' is load current. Equation 14 and 15 are obtained from the plots from 6 and 7 using linear regression analysis.

The generalized mathematical equation for core loss at stator core, rotor core and total core loss is obtained using regression analysis, the resulting the equations of stator core loss, rotor core loss and total core loss of the SCIM are as follows:

Generalized regression equation for stator core loss:

y= 15.778*x - 118.67 (16)

Generalized regression equation for rotor core loss,

y= 0.0281*x - 0.3697 (17)

Generalized regression equation for total core loss,

y= 15.806*x – 119.04 (18)

Here, 'y' gives core loss and 'x' is load current. Equation 16, 17 and 18 are obtained from the plots from Figures 8-10 using linear regression analysis.

The average percentage error between the loss from generalized mathematical equation and the estimated loss from FEM analysis is 1.18% and is tabulated in Table 5. The arrived equations are valid for 160L frame[14].

## 5.0 Thermal Analysis-Lumped Parameter Thermal Model (LPTM)

The temperature of SCIM is predicted using LPTM, and is made up of thermal resistance, capacitance and the heat sources. The conductive resistance is calculated using the geometry and material characteristics. The convective thermal resistance is estimated using the Prandtl and Reynolds values. In this case, the effect of radiation is neglected. Calculated thermal resistance, heat sources, and heat movement at each node is the foundation of the LPTM. Temperature varies with respect to time and is as given by ODE equation (11).

$$\rho C_p V \frac{dT}{dt} = Q_{in} - Q_{out} + Q_{generated} \quad (11)$$

The LPTM has included the heat transfer mechanisms and main elements within the 3ϕ-SCIM. The SCIM is split into lumped elements, having thermal storage and heat generation, interconnecting with nearby components.

The 15kW, 3ϕ-SCIM is divided into main ten components and is shown in Figure 16, the SCIM is symmetrical on its axis.

Since all components are cylindrical, the thermal resistances are now determined using cylindrical lumped components. The convective heat transfer technique is used to determine the thermal resistances of the air gap and end cap air. As shown in Figure 17, the network of ten elements represents the total ten element LPTM of the 15kW, 3ϕ-SCIM.

From the energy balance equation (11), mathematical formulae that describe the thermal behavior of 3ϕ-SCIM are obtained.

### 5.1 Performance of LPTM

In this session, the performance of the 10-element LPTM of the 3ϕ-SCIM is used to evaluate the temperature rise at various nodes using equation (12).

dT = A*T+ u*B (12)

**Table 5.** Rise in temperature at various parts of 3ϕ-SCIM - LPTM

| Element / Load | Considering Constant Core Loss | | | |
|---|---|---|---|---|
| | No-Load | Half Load | 3/4$^{th}$ load | Full Load |
| Stator Core | 24.36 | 28.11 | 61.95 | 95.05 |
| Stator Winding | 23.29 | 27.18 | 61.36 | 94.77 |
| Rotor Winding | 21.41 | 25.41 | 58.70 | 91.28 |
| Rotor Core | 20.98 | 24.93 | 57.97 | 90.31 |

where, 'A' is a conductance matrix, 'B' is a loss matrix, and 'u' is a unity matrix.

The losses in SCIM determines the temperature rise at various load conditions. The estimated temperature rises at various parts of SCIM, at different load conditions considering losses is as presented in Table 2.

The results presented in Table 8 is for major 4 elements (Stator Winding (SW), Stator Core (SC), Rotor Core (RC) and Rotor Winding (RW)) for which the comparison is carried out with LPTM analysis.

## 6.0 Thermal Analysis – 3D Fem Model

The rise in temperature in 3ϕ-SCIM is because of the motor losses. In this research, the variation in temperature is accounted for the loss assessment. A 3D FEM model is developed for evaluation of rise in temperature at various parts of the 3ϕ-SCIM at different load conditions

The 3D model is meshed using the HYPERMESH tool, as seen in Figure 11. Figure 12 illustrates how the generated meshed 3D model looks in the CFD tool, and evaluates the rise in temperature at various part of the SCIM as show in Figure 13. The losses per volume fed to the 3D CFD model and enumerated in Table 4 are used to determine heat sources in SCIM.

The rise in temperature in 3ϕ-SCIM is analyzed using the computational tool ANSYS CFX. Table 6 lists the heat

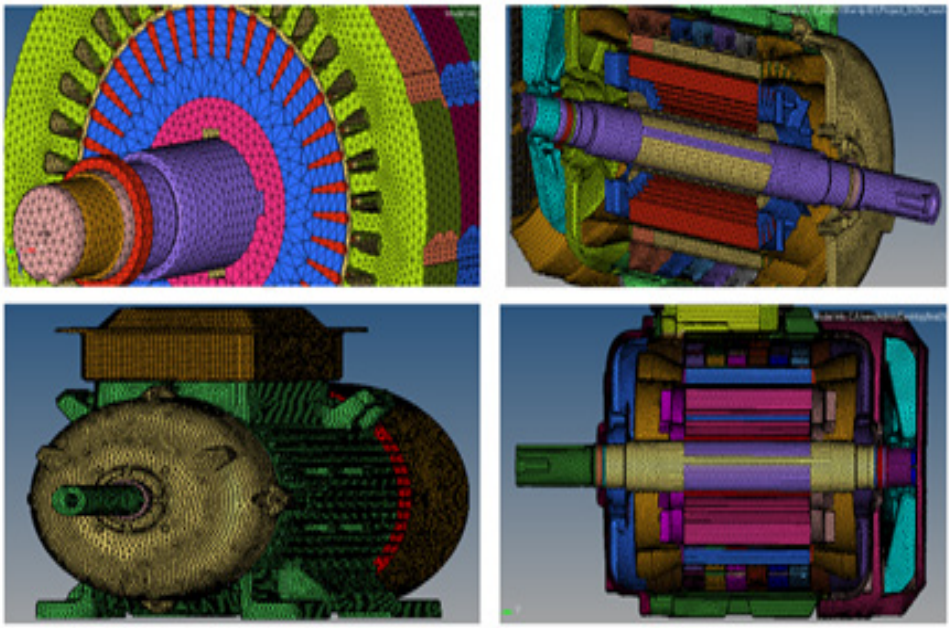

**Figure 11.** Cross section view of overall 2D meshed model with common surface.

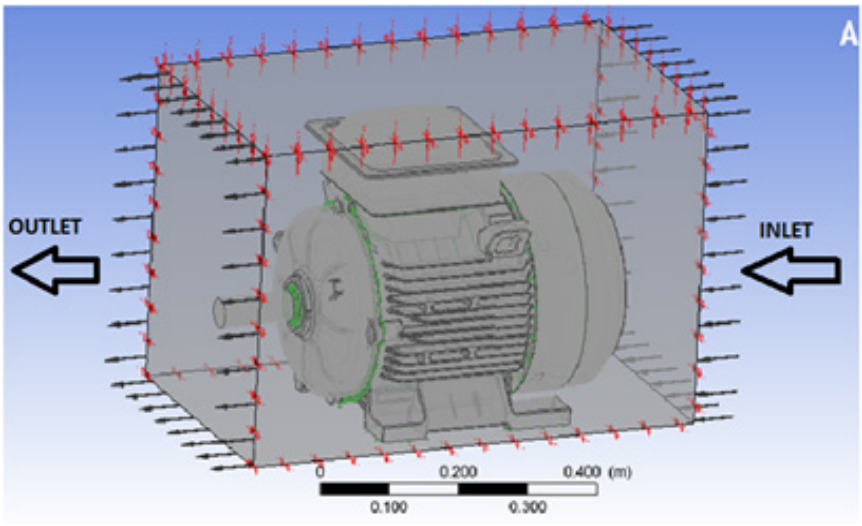


**Figure 12.** Overall CFX Model setup file.

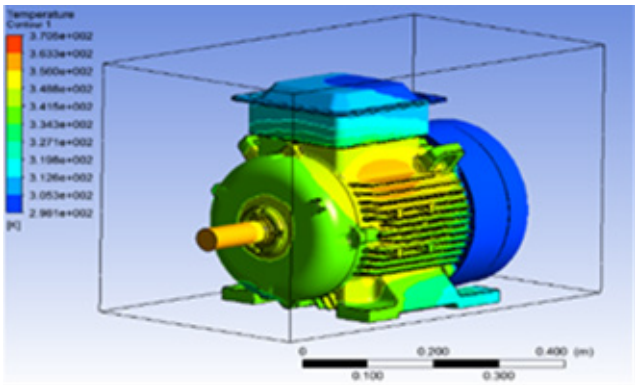

**Figure 13.** Overall temperature distribution in 15 kW SCIM.

sources that were determined for the 15 kW 3ϕ-SCIM. In order to predict the increase in temperature, the 3D-CFD model incorporates the predicted heat sources.

For the 15 kW 3ϕ-SCIM, the temperature increase is calculated at 25$^0$C ambient temperature as shown in Figure 13. The rise in temperature at different load conditions is observed. The temperature rises are maximum at Stator Windings (SW), Stator Core (SC), Rotor Windings (RW), and Rotor Core (RC). Figure 13 depicts the rise in temperature at different parts of SCIM. Figure 14 depicts the distribution of temperature as seen in flat part of the SCIM[17].

**Table 6.** Heat sources of 15 kW SCIM at different loads

| Motor Component | No Load | Half Load | 3/4$^{th}$ Load | Full Load |
|---|---|---|---|---|
| | δ in W/m$^3$ | δ in W/m$^3$ | δ in W/m$^3$ | δ in W/m$^3$ |
| Stator Conductors | 41860 | 63178 | 173643 | 250000 |
| Stator Core | 56795 | 56795 | 56795 | 56795 |
| Rotor Core | 71148 | 71148 | 71148 | 71148 |
| Rotor Bars (each) | 462 | 4759 | 7388 | 9629 |

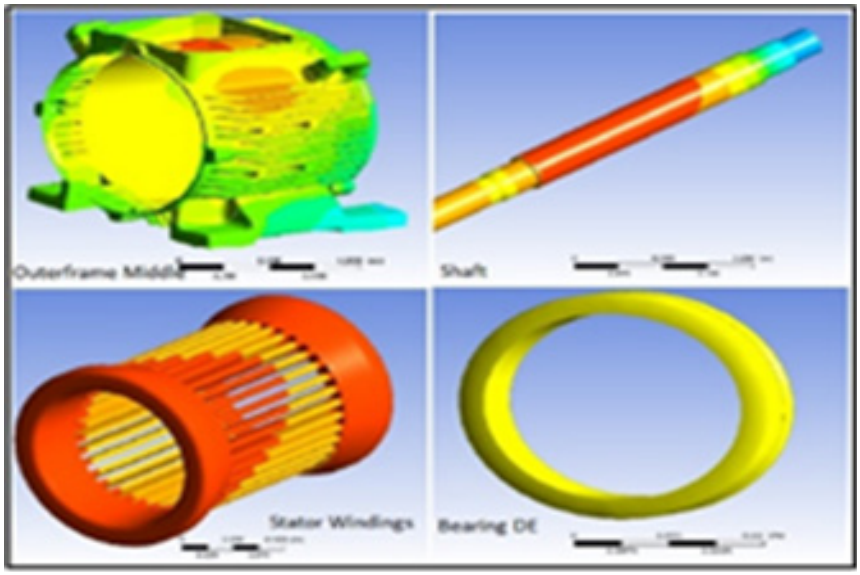


**Figure 14.** Temperature at various parts of motor.

### 6.1 Temperature Rise in SCIM

The temperature rise at various part of the 15-kW 3ϕ-SCIM are as given in Table 7 using FEM and is as shown in Figure 13 and Figure 15.

## 7.0 Comparative Analysis

The estimated temperature considering LPTM and FEM in Stator Winding (SW), Stator Core (SC), Rotor Core (RC) and Rotor Winding (RW) is as plotted in Figures 18-21, respectively.

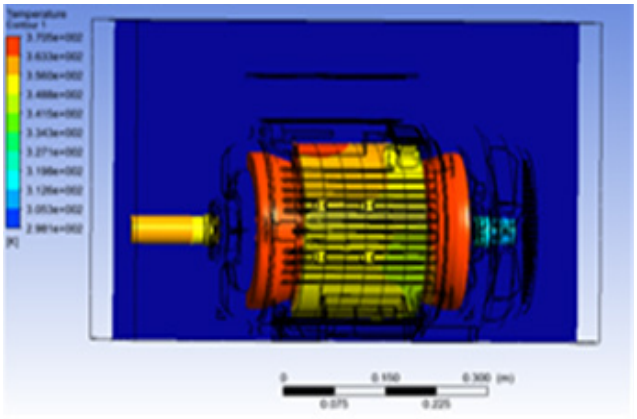

**Figure 15.** Temperature distribution in plane section of the motor.

**Table 7.** Rise in temperature at various parts of 3ϕ-SCIM – 3D-FEM model

| Motor Component | Rise in Temperature ($^0$C) | | | |
|---|---|---|---|---|
| | No Load | Half Load | ¾$^{th}$ Load | Full load |
| Stator Winding (SW) | 29.55 | 35.31 | 51.15 | 68.15 |
| Stator Core (SC) | 23.57 | 30.08 | 44.23 | 58.46 |
| Rotor Core (RC) | 27.17 | 34.63 | 49.52 | 65.74 |
| Rotor Windings (RW) | 26.87 | 34.28 | 49.64 | 65.36 |

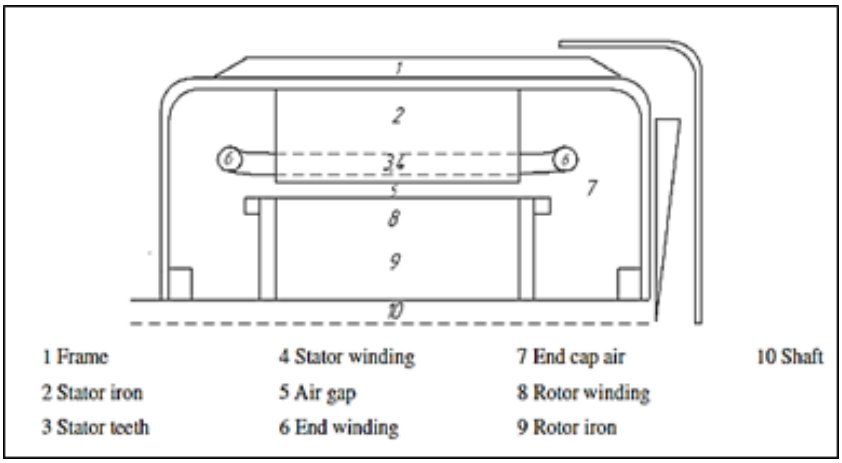


**Figure 16.** Ten elements considered to develop LPTNM[4].

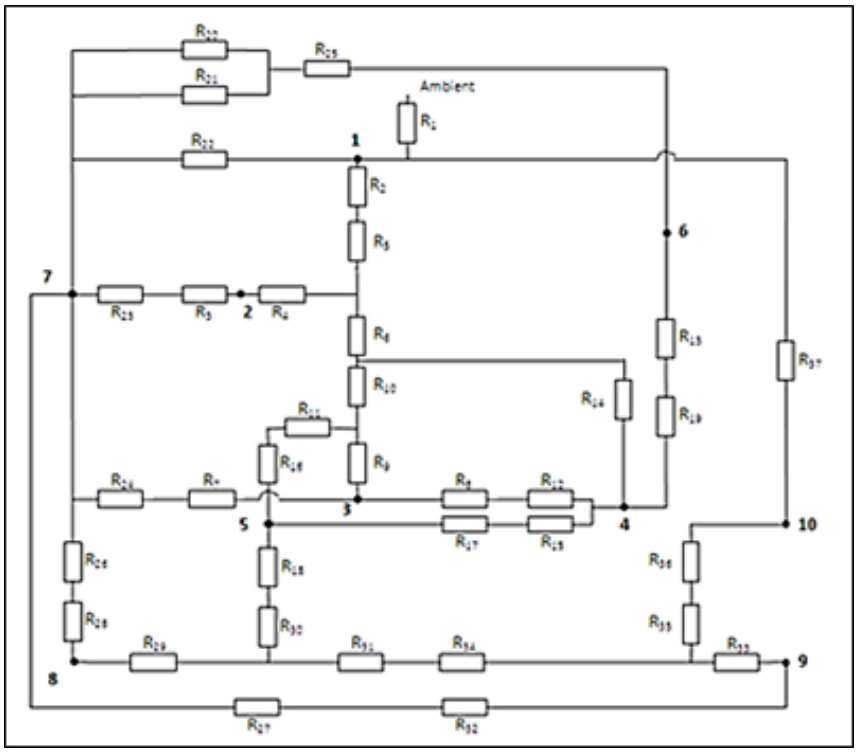


**Figure 17.** Ten Element LPTM of SCIM[4].

In all the plots X-axis is Load and Y-axis is temperature rise. The plots of Load vs. temperature rise it is evident that the FEM analysis is yielding more reliable results. LPTM uses Ordinary Differential Equations (ODE) and is solved using state space variable technique. LPTM is a 1D system comprising of thermal resistances, which is only dependent on material and geometry of the SCIM. LPTM is a linear system as it used ODE.

FEM analysis uses Partial Differential Equations (PDE), and is nonlinear system. PDE's are solved using numerical techniques with convergence accuracy of $1x10^{-4}$. Hence the results of FEM analysis are more

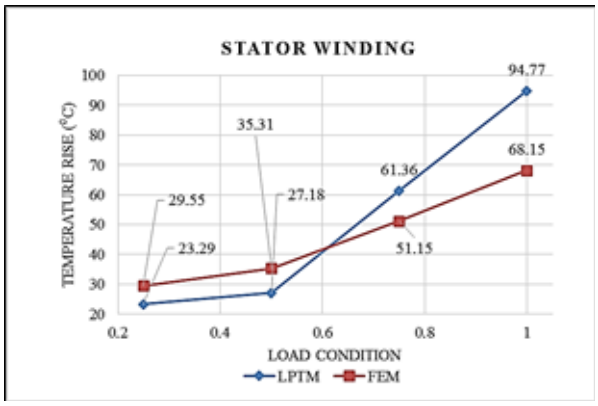


**Figure 18.** Stator core temperature rise.

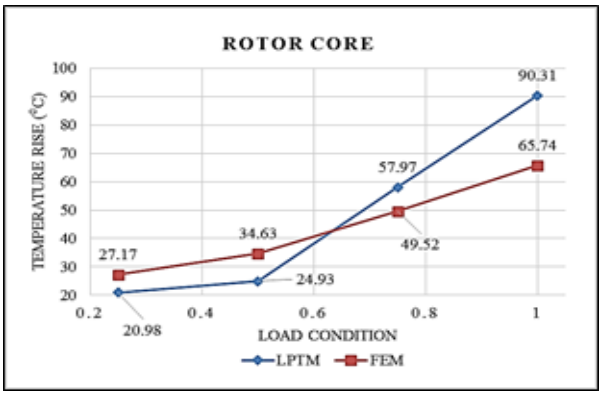


**Figure 20.** Rotor core temperature rise.

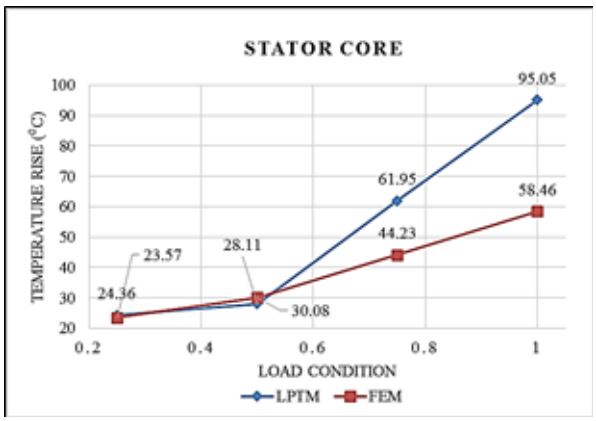


**Figure 19.** Stator core temperature rise.

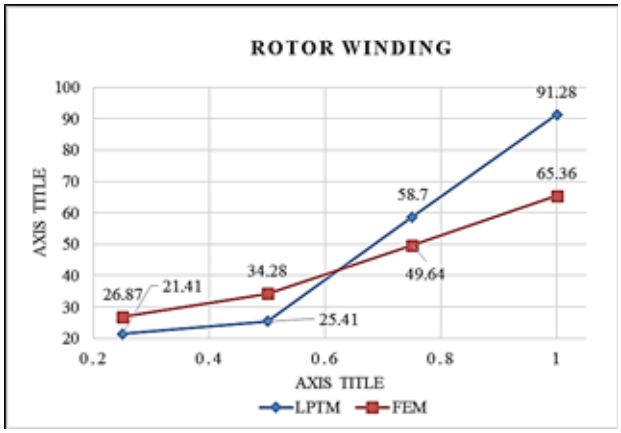


**Figure 21.** Rotor winding temperature rise.

**Table 8.** Relative % error between LPTM and FEM

| Load Condition | Temperature Rise (°C) | | | |
|---|---|---|---|---|
| | No-Load | Half Load | 3/4th Load | Full Load |
| SW-LPTM | 23.29 | 27.18 | 61.36 | 94.77 |
| SW-FEM | 29.55 | 35.31 | 51.15 | 68.15 |
| % error | 21.18 | 23.02 | -19.96 | -39.06 |
| SC-LPTM | 24.36 | 28.11 | 61.95 | 95.05 |
| SC-FEM | 23.57 | 30.08 | 44.23 | 58.46 |
| % error | -3.35 | 6.55 | -40.06 | -62.59 |
| RC-LPTM | 20.98 | 24.93 | 57.97 | 90.31 |
| RC-FEM | 27.17 | 34.63 | 49.52 | 65.74 |

| | | | | |
|---|---|---|---|---|
| % error | 22.78 | 28.01 | -17.06 | -37.37 |
| RW-LPTM | 21.41 | 25.41 | 58.7 | 91.28 |
| RW-FEM | 26.87 | 34.28 | 49.64 | 65.36 |
| % error | 20.32 | 25.88 | -18.25 | -39.66 |

reliable than LPTM. ANSYS Maxwell tool is used to carry out FEM analysis. MATLAB is used to carry out LPTM analysis. The relative % error between LPTM and FEM analysis and is as tabulated in Table 8.

## 8.0 Conclusion

A LPTM and FEM is constructed for the thermal analysis of 15kW 3ϕ-SCIM. The motor's steady-state temperature can be determined analytically using the LPTM model at the early stages of construction or design. Most 3ϕ-SCIM can be simply fitted with the model. However, due to many simplifications, the LPTM model's accuracy is limited. LPTM is designed for 15kW 3ϕ-SCIM in this case and temperature rise is obtained at various load conditions. Similarly, 3D model is developed for 15kW 3ϕ-SCIM and thermal analysis is carried out using FEM with convergence accuracy of $1x10^{-4}$. Results of temperature rise at Stator Winding (SW), Stator Core (SC), Rotor Core (RC), and Rotor Winding (RW) are plotted. Relative % error is calculated. Analysis concluded that FEM analysis yields better and reliable results than LPTM.

## 9.0 References


1. Bousbaine A. An investigation into the thermal modelling of induction motors (Doctoral dissertation, University of Sheffield).
2. Hooli SS, Vadde A, Manickavasagam K, Kadambi GR. Measurement of torque using leakage flux for induction motors in electric vehicles by non-invasive method. Innovations in Electrical and Electronic Engineering: Proceedings of ICEEE 2020. Singapore: Springer; 2021. p. 489-503. https://doi.org/10.1007/978-981-15-4692-1_38
3. Khazi S, Vadde A, Manickavasagam K, Kadambi GR, Narayanan V, Lokesh BM, *et al.* Analyzation of temperature rise in induction motor for electric vehicles. Advances in Energy Technology: Select Proceedings of EMSME 2020. Singapore: Springer; 2022. p. 173-83. https://doi.org/10.1007/978-981-16-1476-7_17
4. Hooli SS, Vadde A, Manickavasagam K, Kadambi GR. Fuzzy based health monitoring of electric vehicle motor using time domain analysis. 2021 International Conference on Sustainable Energy and Future Electric Transportation (SEFET); 2021. p. 1-6. https://doi.org/10.1109/SeFet48154.2021.9375791
5. Sudha B, Vadde A, Manickavasagam K, Kadambi. Characterization of temperature and productive torque for 160L frame squirrel cage induction motor. EMSME; 2020. https://doi.org/10.36909/jer.EMSME
6. Nasir BA. An accurate iron core loss model in equivalent circuit of induction machines. J Energy. 2020; 2020. https://doi.org/10.1155/2020/7613737
7. Bašić M, Vukadinović D, Polić M. Stray load and iron losses in small induction machines under variable operating frequency and flux: A simple estimation method. IEEE Trans Energy Convers. 2017; 33(2):869-76. https://doi.org/10.1109/TEC.2017.2759816
8. Gmyrek Z, Boglietti A, Cavagnino A. Estimation of iron losses in induction motors: Calculation method, results, and analysis. IEEE Trans Ind Electron. 2009; 57(1):161-71. https://doi.org/10.1109/TIE.2009.2024095
9. Stenglein E, Kuebrich D, Albach M, Duerbaum T. Novel fit formula for the calculation of hysteresis losses including DC-premagnetization. PCIM Europe. 2019 International Exhibition and Conference for Power Electronics, Intelligent Motion, Renewable Energy and Energy Management; 2019. p. 1-8.
10. Sachin S, Sriram AT. Review of physical and mathematical modelling aspects of thermal management of induction motors. J Phys Conf Ser. 2020; 1706(1). https://doi.org/10.1088/1742-6596/1706/1/012105
11. Hooli SS, Vadde A, Manickavasagam K, Kadambi GR. Measurement of torque using leakage flux for induction motors in electric vehicles by non-invasive method. Innovations in Electrical and Electronic Engineering: Proceedings of ICEEE 2020. Singapore: Springer; 2021. p. 489-503. https://doi.org/10.1007/978-981-15-4692-1_38

12. Mynarek P, Kowol M. Thermal analysis of three-phase induction motor using circuit models. Electrodynamic and Mechatronic Systems; 2011. p. 119-22. https://doi.org/10.1109/SCE.2011.6092137
13. Staton D, Boglietti A, Cavagnino A. Solving the more difficult aspects of electric motor thermal analysis in small and medium size industrial induction motors. IEEE Trans Energy Convers. 2005; 20(3):620-8. https://doi.org/10.1109/TEC.2005.847979
14. Sudha B, Vadde A, Manickavasagam K. Thermal behavior on productive torque in electric vehicle motor using computational methods. 2021 IEEE 6th International Conference on Computing, Communication and Automation (ICCCA); 2021. p. 367-371.
15. Sudha B, Vadde A, Manickavasagam K, Kadambi GR. Characterization of temperature and productive torque for 160L frame squirrel cage induction motor. J Eng Res. 2021:35-46.
16. Sachin S, Manickavasagam K, Sriram AT. Effect of the temperature fluctuation on torque production by assimilating variable core loss using computational approach for electric vehicles motors. Int Rev Electr Eng. 2022; 17(6). https://doi.org/10.15866/iree.v17i6.22503
17. Sachin S, Manickavasagam K, Sriram AT. Effect of core losses on thermal analysis of 3ϕ-squirrel cage induction motor using lumped parameter thermal model. Mater Today Proc. 2023; 80:724-30. https://doi.org/10.1016/j.matpr.2022.11.076